DOI: 10.26599/FSHW.2026.9250941

Contents lists available at SciOpen

Food Science and Human Wellness

journal homepage: https://www.sciopen.com/journal/2097-0765

China Food Publishing Co.

Artemisia capillaris Thunb. Tea Alleviates HFD -induced Obesity in Micethrough Modulating the Gut-liver Axis

Yi Guo [1#], Weiting Han [1#], Xiao Xiao [1], Meng Liang [1], Lv Meiwei[1], Yu Wang [1], Xiaowen Jiang [1*], Wenhui Yu [1,2,3*]

[1] *College of Veterinary Medicine, Northeast Agricultural University, Harbin, 150030, China*

[2] *Institute of Chinese Veterinary Medicine, Northeast Agricultural University, Harbin, 150030, China*

[3] *Key Laboratory for Prevention and Treatment of Common Animal Diseases in Heilongjiang Province General Universities, Harbin, 150030, China*

ABSTRACT: Obesity is a prevalent chronic metabolic disorder. Artemisia capillaris Thunb., a natural plant known for its hepatoprotective and choleretic properties, is commonly brewed into Artemisia capillaris Thunb. tea (ACTE). Artemisia capillaris Thunb. rich in a variety of bioactive constituents, including organic acids, coumarins, and essential oils, which contribute to its therapeutic potential in liver health. This study evaluates the potential therapeutic effects of ACTE in a high-fat diet (HFD)-induced obese murine model by observing mouse phenotypes, conducting biochemical analyses, performing 16S rRNA gene sequencing, utilizing bile acid-targeted metabolomics, and applying molecular biology techniques to comprehensively explore the mechanisms of ACTE. The results demonstrate that ACTE ameliorates obesity and hepatic lipid accumulation in obese mice, modulates gut microbiota composition, activates the FXR signaling pathway, enhances bile acid enterohepatic circulation, strengthens intestinal barrier integrity, and alleviates liver inflammation and pyroptosis by inhibiting the NF-κB and NLRP3 signaling pathways. These findings suggest that ACTE ameliorates HFD-induced obesity in mice by modulating the gut–liver axis through interactions between the gut microbiota and its metabolites, providing a new way of eating to improve human health.

Keywords: Artemisia capillaris Thunb.; Obesity; Gut microbiota; Bile acid; Lipid metabolism

1. Introduction

Obesity ranks among the most prevalent chronic metabolic disorders globally and, if not properly managed, can advance to metabolic dysfunction-associated steatotic liver disease (MASLD), which now represents the leading form of chronic liver disease, impacting up to 38% of adults worldwide. Such a high prevalence poses a significant challenge to public health systems [1, 2]. The onset of obesity is closely associated with prolonged intake of poor dietary patterns rich in cholesterol (CHO) and free fatty acids (FFA), leading to hepatic lipid metabolism disorders and abnormal fat accumulation. It is often accompanied by complications such as insulin resistance, hypertension, and inflammation, ultimately progressing to

[#]Co-first authorship
***Co-Correspondence**
Wenhui Yu (yuwenhui@neau.edu.cn)
Xiaowen Jiang (jiangxiaowen@neau.edu.cn)

Received 23 April 2025
Received in revised from 17 July 2025
Accepted 2 December 2025

multi-system diseases [3, 4]. Therefore, exploring the molecular mechanisms of obesity and identifying safer and more effective intervention strategies are crucial.

Bile acids (BAs), as key molecules regulating lipid digestion and absorption, play a dual role in metabolic processes. They emulsify fats, increasing their surface area for interaction with lipases, thus accelerating lipid hydrolysis and metabolism [5]. In the liver, CHO is transformed into primary BAs by cytochrome P450 enzymes [6]. The bile salt export pump (BSEP) transports BAs into the gallbladder, from where they are discharged into the duodenum via the bile duct. Approximately 95% of BAs are absorbed back by the apical sodium-dependent BA transporter (ASBT) in the ileal enterocytes [7, 8], where they bind to the ileal BA-binding protein (IBABP), which mitigates the toxicity of BAs to cells. Subsequently, BAs are exported into the bloodstream via the heterodimeric transporters Ostα/β. The conjugated BAs (conj. BAs) are then transported into the liver by the sodium taurocholate cotransporting polypeptide (NTCP), initiating a new round of enterohepatic circulation [9, 10].

Obesity development and advancement are closely associated with the vital connection between intestinal and hepatic functions. The composition of BAs can be altered by gut microbiota. Furthermore, an imbalance in the gut microbiota results in heightened permeability of the intestinal mucosa. [11]. Lipopolysaccharide (LPS), a detrimental byproduct produced by gut microbiota, can be transported to the liver through the circulatory system. Upon arrival, it can stimulate the TLR4/NF-κB signaling pathway, resulting in the excessive secretion of pro-inflammatory cytokines [12], initiating the activation of inflammasomes, particularly activating the NLRP3/caspase-1 pathway, ultimately inducing cellular pyroptosis.

Artemisia capillaris Thunb. (abbreviated as Yin Chen Hao)is a natural herb widely distributed in Southeast Asia, mainly located in China, Malaysia, Japan and other countries [13]. A. capillaris Thunb. is often finely chopped and consumed raw, incorporated into flour to make pancakes or porridge, or decocted and cooked with rice to prepare congee. Its water-based extract, known as A. capillaris Thunb. Tea (ACTE), has traditionally been applied in clinical practice to manage diseases related to the liver and gallbladder, with definite choleretic, antipyretic, and lipid-lowering efficacies. Contemporary research in pharmacology has demonstrated that coumarins in A. capillaris Thunb. can induce the expression of BAs transporter proteins, promote bile secretion, and help to alleviate jaundice symptoms caused by cholecystitis, gallstones, etc. Organic acid compounds, such as caffeic acid and chlorogenic acid in A. capillaris Thunb., can change the permeability of the bacterial outer membrane, regulate the intestinal flora and participate in the microbial energy competition [14, 15].

Therefore, we firstly elucidated the effective bioactive components of ACTE by LS-MS/MS and assessed the intervention effect of ACTE on HFD-induced obesity in mice by mouse signs and lipid biochemical parameters. Combined with 16S rRNA gene sequencing and BA-targeted metabolomics techniques to analyze the composition of mouse gut microbiota, BA metabolic pathways, and inflammatory and pyroptotic responses, we explored the molecular mechanisms by which ACTE intervened in mouse

obesity. These findings offer potential clues regarding the anti-obesity properties of ACTE and shed light on its lipid-reducing mechanisms through modulation of the gut–liver axis.

2. Materials and methods

2.1 Experimental Material

A. capillaris Thunb. was purchased from Song Shan Tang Pharmaceutical Company (Harbin, China). Kits for measuring alanine aminotransferase (ALT), aspartate aminotransferase (AST), Creatinine (Cr), Blood Urea Nitrogen (BUN), total cholesterol (TC), triacylglycerol (TG), low-density lipoprotein (LDL), and high-density lipoprotein (HDL), as well as TBA kits, were obtained from the Nanjing Jian Cheng Bioengineering Institute in Nanjing, China. Furthermore, Bile salt hydrolase (BSH) and LPS ELISA kits were procured from Jing Mei Biotechnology Institute in Jiangsu, China.

2.2 Extraction and Preparation of ACTE

A total of 100 g of dried A. capillaris Thunb. was weighed, and 1000 mL of distilled water was added. The mixture was left undisturbed at ambient temperature for 30 mins, followed by a 1h boiling process to acquire the primary extract. Following this, 800 mL of distilled water was introduced to the leftover plant material, and the decoction procedure was carried out again for 1h. The two collected decoctions were then combined, filtered, and centrifuged to remove insoluble substances. The resulting liquid was concentrated to 100 mL and lyophilized at -50℃. The average yield of ACTE was 20.28% (w/w).

2.3 Animal Grouping and Husbandry Conditions

A total of 42 male C57BL/6 mice (5 weeks old, 20 ± 2.5 g; Liaoning Changsheng Biological Co., Ltd.) were housed under standardized conditions (25 ± 1℃, 45% ± 5% humidity) with ad libitum access to food and water. All experimental protocols involving animals received ethical approval from the Northeast Agricultural University Animal Testing Ethics Committee (No. NEAUEC-20210119). Upon completion of a one-week adaptation phase, the animals were allocated into six experimental groups in a random manner, including a normal diet group (ND) and a group receiving a ND plus A. capillaris Thunb. extract (ND+ACTE), both maintained on standard chow. Moreover, mice assigned to the high-fat diet group (HFD), the positive control group (PC), the low-dose ACTE treatment group (ACTE-L), the middle-dose ACTE treatment group (ACTE-M/HFD+ACTE), and the high-dose ACTE treatment group (ACTE-H) were fed a HFD (D12492, Komibi Yutai Biotechnology Co. Ltd., Beijing, China) for 16 weeks(n=6). The nutritional composition of the HFD is shown in Supplementary Table S1. Following successful obesity model induction at week 16, mice in PC group received oral administration of atorvastatin calcium tablets at a dose of 10 mg/kg/day (Dongrui Pharmaceutical Co., Ltd., Fujian, China). Meanwhile, mice in the ACTE-L, ACTE-M, and ACTE-H groups were orally administered ACTE administered at daily doses of 25, 50, and 75 mg/kg, respectively. The ND+ACTE group was given ACTE at 50 mg/kg/day. The drug doses were selected based on screening in preliminary experiments and supported by prior research results from our group[16]. In contrast, mice in both the ND and HFD groups received an equivalent volume of double-distilled water by gavage, in order to

control for the potential impact of the gavage procedure itself. All treatments were conducted twice weekly for a total duration of six weeks. Body weight and food consumption were tracked on a weekly basis, and feces were collected 48 hours after the last administration of the drug. Before dissection, mice underwent a 12-hour fast, were anesthetized with ether, and blood was sampled from the orbital sinus. The liver, epididymal white adipose tissue (eWAT) and ileum were collected and measured for weight. Blood samples centrifuged to separate the serum.

2.4 Biochemical kit and ELASA kit detection

Serum levels of AST, ALT, Cr, BUN, TG, TC, LDL, and HDL; liver levels of TC and TG; and TBA in hepatocytes, ileal epithelial cells, and fecal samples were analyzed with biochemical kits following the instructions. Levels of BSH and serum LPS in fecal bacterial fluid were measured using the Mouse Protein ELASA Kit, as per the protocol provided by the manufacturer.

2.5 Histopathological observations

Liver and ileum tissues were preserved in 4% paraformaldehyde, subjected to dehydration in a series of alcohol solutions, embedded in paraffin, and then sectioned. Histological alterations in the liver and ileum were examined using hematoxylin and eosin (H.E.) staining. Oil Red O staining was conducted to detect lipid droplet buildup in hepatocytes.

2.6 qRT-PCR Analysis of Transcript Levels of Related Genes

Total RNA from the liver and ileum was isolated using the kit provided by Magen Biotech (Guangzhou, China), following the manufacturer's guidelines. RNA levels were assessed, followed by reverse transcription into cDNA utilizing a kit from Bioer Technology (Hangzhou, China). The relative expression levels of genes were assessed by real-time fluorescence quantitative qPCR method. A Roche 480 qPCR instrument (Roche Diagnostics, Mannheim, Germany) was used for amplification experiments. The amplification protocol began with a 10mins denaturation at 95℃, followed by 40 cycles consisting of 15s at 95℃ and 1min at 60℃. Relative mRNA expression levels were determined by normalizing to β-actin protein as an internal control, with calculations made using $2^{-\Delta\Delta Ct}$ method. Primer design details are provided in Supplemental Table S2.

2.7 Western blot Analysis of Relevant Protein Expression Levels

Tissues were lysed with RAPI protein lysate and quantified by BCA protein assay kit (meilunbio, Dalian, China). The extracted total proteins were mixed with buffer and boiled to prepare protein samples to be assayed. The target protein was separated via SDS-PAGE, then the corresponding molecular weight region was excised and transferred to a PVDF membrane, which was blocked with skimmed milk at ambient temperature for 1h. Incubate the primary antibody after blocking. Following incubation, the membrane was washed and then incubated with the secondary antibody for 1h at ambient temperature. Antibody dilution ratios and sources are listed in Table S3. The ECL luminescence reagent (Meilunbio, Dalian, China) was used to develop the chemiluminescent signal, and the protein bands were visualized using a bioimaging system

(Clinx Science Instruments, Shanghai, China). The gray values of the chromogenic protein bands were compared to those of the internal reference gene, β-actin.

2.8 ACTE Main Component Analysis

Weigh the sample, add 600 μL of MeOH (with 2-chloro-L-phenylalanine at 4 ppm), vortex, and then grind for 60s. Sonicate the sample at ambient temperature for 15mins, centrifuge at 12,000 r/min and 4℃ for 10mins, and filter the supernatant before LC-MS/MS analysis. The conditions for liquid chromatography and mass spectrometry are detailed in the Supplementary Material.

2.9 Non-labeled quantitative proteomic analysis of the liver

The experiments were performed by Parsonage (Nanjing, China). A sufficient quantity of protein was extracted from the sample, trypsinized using the Filter-Aided Proteome Preparation technique, desalted using a C18 cartridge, lyophilized, and re-dissolved in 40 μL of dissolution buffer, followed by quantification via OD280. The conditions for liquid chromatography and mass spectrometry can be found in the Supplementary Information. The corresponding data were retrieved using Maxquant software. GO annotation and KEGG pathway annotation of the target protein collection were performed using the software Omicsbean (http://www.omicsbean.cn/).

2.10 Targeted metabolomic analysis of BAs

Mouse cecum content was accurately weighed, followed by mixed internal standard working solution and 20% methanol acetonitrile solution. After vortexing and centrifugation, the supernatant was collected and subjected to concentration. BAs in mouse cecum contents were quantified using Ultra Performance Liquid Chromatography (UPLC) (ExionLC™ AD) coupled with Tandem Mass Spectrometry (MS/MS) (QTRAP®6500+). Different concentrations of standard solutions were prepared by 2-fold dilution of 1000 ng/mL standard solution to 0.1 ng/mL in order to establish standard curves for various compounds. The information on BA standard substances and the linear equations of standard curves are shown in Supplementary Table S7. The conditions for liquid chromatography and mass spectrometry are detailed in the Supplementary Material. Based on the quantitative results, relevant data analysis was performed. The chromatographic and mass spectrometric conditions are provided in the supplementary file. A database was constructed using standard compounds to conduct qualitative and quantitative analysis of the mass spectrometry data. XCMS software was employed for data preprocessing to remove background noise and quantify metabolites across different groups.

2.11 Gut Microbiota 16S rRNA sequencing analysis

This experiment was performed by Parsonage Genetics Technology Co Ltd (Nanjing, China). A total of 0.5 g of cecum contents from each mouse group was accurately weighed and added to a centrifuge tube containing extraction lysate for grinding. The OMEGA Soil DNA Kit (M5635-02; Norcross, GA, USA) was employed for nucleic acid extraction. Simultaneously, DNA was quantified by Nanodrop. The 16S rDNA V3 and V4 variable regions were amplified using specific primers: 338F

(5'-ACTCCTACGGGGAGGCAGCA-3'), 806R (5'-GGACTACHVGGGGTWTCTAAT-3'). Quantification of PCR products was performed on a Microplate reader (BioTek, FLx800) using Quant-iT PicoGreen dsDNA Assay Kit. Sequencing libraries were prepared using the TruSeq Nano DNA LT Library Prep Kit from Illumina (NEB, USA), and the quality of the libraries was assessed using an Agilent Bioanalyzer 2100 and a Qubit@ 2.0 Fluorometer (Thermo Scientific) before loading. Sequencing was performed on the Illumina NovaSeq 6000 platform, producing paired-end reads of 250 bp. Species taxonomic annotation, taxonomic composition analysis, Alpha diversity analysis, and Beta diversity analysis were performed on our obtained ASV feature sequences using QIIME2 and selecting the Greengenes database.

2.12 Molecular Docking

The appropriate protein structure of the molecular docking gene FXR (Q96RI1) was queried in the Uniprot database. The 3D structure files in SDF format of ACTE effective bioactive components were obtained from the PubChem database (https://pub chem.ncbi.nlm.nih.gov/). Molecular docking was conducted using AutoDock Vina with AutoDock Tools. Molecular docking results were visualized using Pymol. The interaction forces between the protein and the small molecule were analysed using Ligplot.

2.13 IHC staining

Xylene pairs were used to deparaffinize the tissue sections, followed by treatment with ethanol at gradually decreasing concentrations, and rinsed under running water. The tissue sections were then incubated with freshly prepared hydrogen peroxide, rinsed, and subjected to antigen retrieval using citrate buffer solution. After blocking, the sections were incubated with the primary antibody against FXR at 4℃ overnight, followed by incubation with a secondary antibody. The DAB working solution was applied, and after staining, hematoxylin staining solution was added. The sections were then rinsed with running water. The degree of nuclear staining was observed under a light microscope to assess whether the staining intensity met the required standard.

2.14 Statistical Analysis

All results are presented as the form of mean ± standard deviation (Mean ± SD). Statistical analyses were conducted using SPSS 27.0 software, and bar graph results were plotted using GraphPad Prism 9.0 software. Statistical tests included repeated measures two-way ANOVA, one-way ANOVA test, or Student's-t test. Statistical significance is denoted by different letters ($P < 0.05$).

3. Resuits

3.1 LC-MS/MS Analysis of ACTE

We used LC-MS/MS to detect the chemical composition of ACTE, and identified the chemical structure of the sample by matching the primary precise mass and secondary fragment spectrogram infor-mation of the compound in the local standard database. As depicted in Fig. 1A/B, the base peak chromatogram (BPC) of positive and negative ions in ACTE revealed the co-identification and labeling of 21 compounds, including (1) Coumarin, (2) (-)-Thebaine(-)-, (3) Chlorogenic acid, (4) trans-Chlorogenic acid, (5) Coumaroylquinic acid,

(6) Isoquercitrin, (7) 5-Hydroxycoumarin, (8) Artemisinic aldehyde, (9) Geranial, (10) Sorbitol, (11) Artemisinic, (12) Quinic acid, (13) Cryptochlorogenic acid, (14) Scopolin, (15) 4-Hydroxybenzoic acid, (16) 3,4-Di-O-caffeoylquinic acid, (17) Chrysosplenetin, (18) Narirutin, (19) Paspalinine, (20) Kaempferol, (21) Isorhamnetin. These peaks were confirmed by their shapes and vali-dated using secondary spectra (Fig. S1). The active ingredients detailed in earlier reports were present in the ACTE samples utilized in this research[16, 17]. Fig. 1C display the 2D structural diagram of the active ingredient in ACTE. The mass-to-charge ratio, retention time, ppm, precursor type, and relative peak areas of the ACTE active ingredients are shown in Table S4.

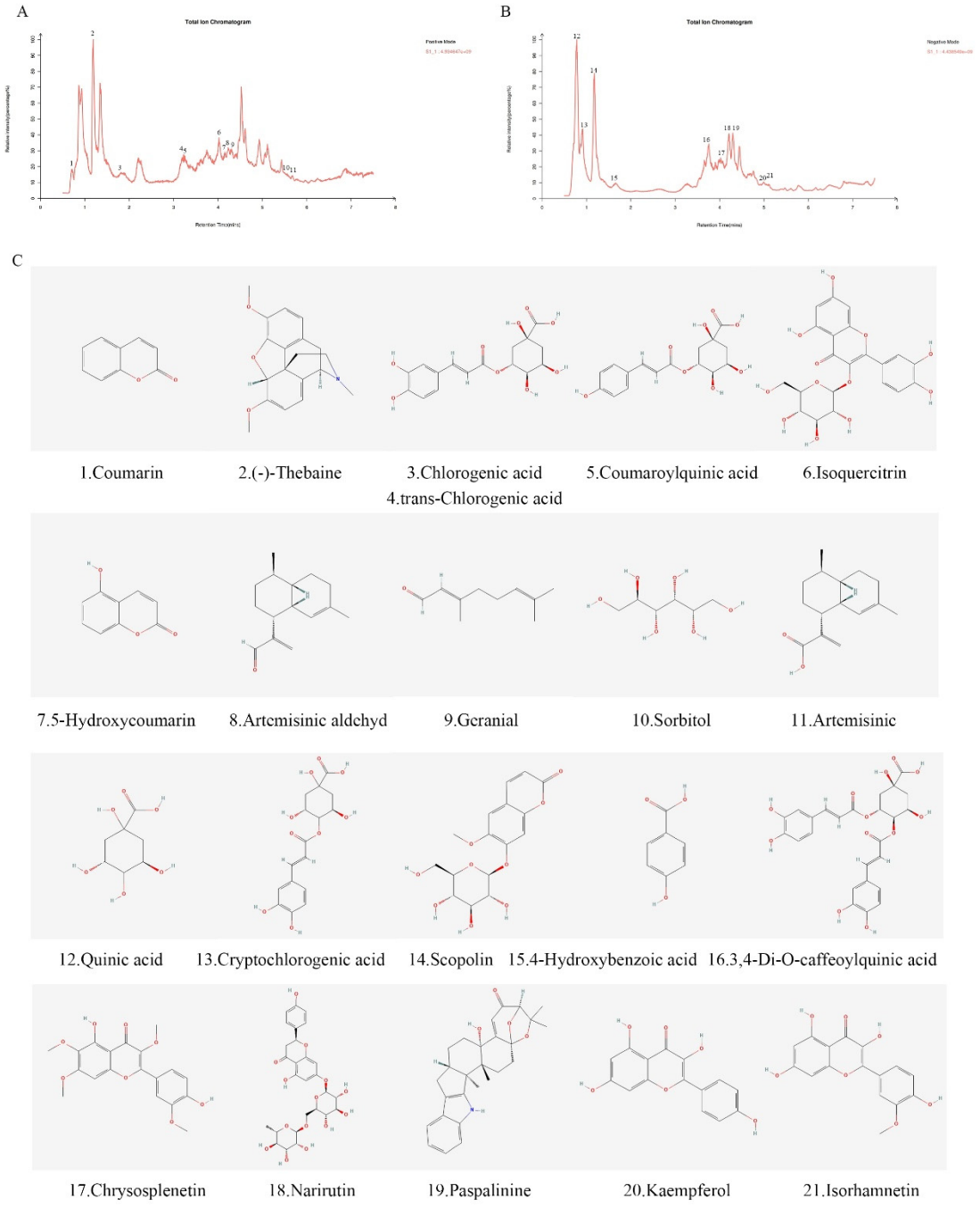

Fig. 1. LC-MS analysis of ACTE. (A) Positive ion mode TIC diagram; (B) Negative ion mode TIC diagram; (C) Active ingredient 2D structural formula.

3.2 ACTE Attenuates Accumulation in HFD-Induced Obese Mice

The experimental design and animal grouping are illustrated in Fig. 2A. Mice in the HFD group had significantly higher final body weight, body weight gain, eWAT and liver weight compared to those in the ND group (Fig. 2B-E/H). After continuous treatment with Atorvastatin calcium tablets and ACTE, mice in the PC and ACTE-L/M/H groups began to lose weight from week 16 onward. The final body weight, body weight gain, eWAT and liver weight of these mice were significantly lower compared to those in the HFD mice. Specifically, the final body weight, eWAT and body weight gain of the mice in the ACTE-M group were significantly lower than those in the ACTE-L and ACTE-H groups, with no significant difference between the ACTE-M group and the ND or PC groups. Food consumption and energy intake did not differ significantly among the HFD groups, indicating that the experimental outcomes were unlikely due to variations in energy intake (Fig. 2F/S2A). As shown in Fig. 2G, ACTE treatment effectively reversed HFD-induced liver yellowing and hypertrophy. Hepatic H.E. staining revealed severe steatosis, disrupted hepatic architecture, and evident hepatocellular hypertrophy, along with diffuse, variably sized round lipid droplets and ballooning degeneration in some hepatocytes. In contrast, the PC and ACTE treatment groups showed reduced hepatic swelling, improved cellular architecture, and alleviated steatosis. However, notable inflammatory infiltration observed in the PC group but not in the ACTE-M group suggests that medium-dose ACTE may be a safer and more effective therapeutic alternative to atorvastatin calcium tablets (Fig. 2G). Oil red O staining results (Fig. 2G/I) indicated that hepatocytes in the HFD group contained numerous diffuse red lipid droplets, indicative of lipid deposition. In comparison, the area of lipid droplets in the PC group and the ACTE treatment group decreased, and the area of lipid droplets in the ACTE-M group was the smallest. Compared with the ACTE-L and PC groups, the ACTE-H group showed a markedly reduced level. There was no difference between ACTE-L and PC. Furthermore, analysis of the drug control group revealed no significant differences in the aforementioned lipid metabolism parameters between the ND+ACTE groups and the ND groups, suggesting that ACTE has no adverse effect on lipid metabolic function in healthy mice under normal physiological conditions. In conclusion, ACTE treatment alleviated obesity signs, reduced hepatic steatosis and liver injury, and decreased hepatic lipid accumulation in obese mice. The most significant therapeutic effect was seen in the middle dose of ACTE.

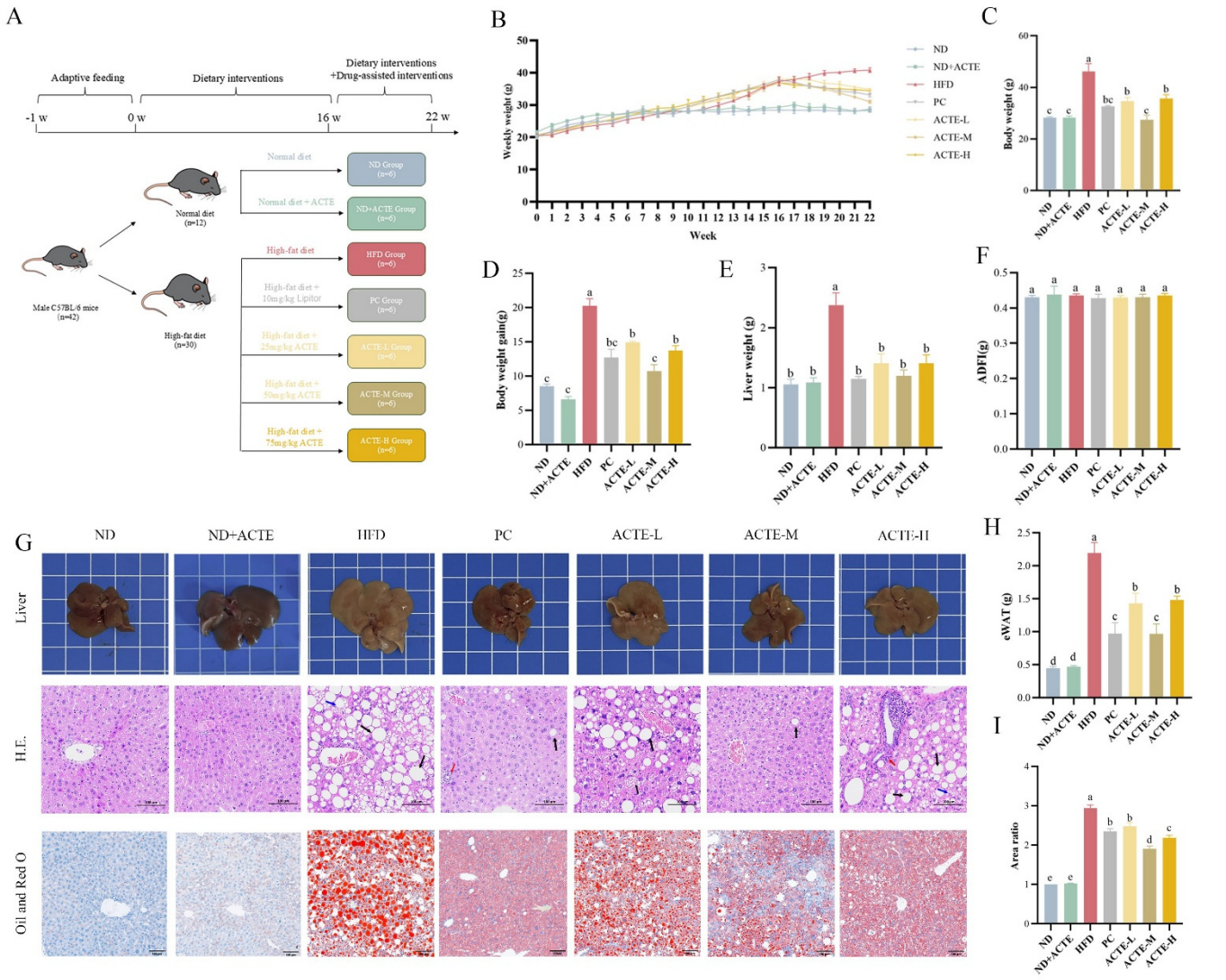

Fig. 2. ACTE improves obesity signs and hepatic lipid accumulation in obese mice. (A) Grouping and feeding of experimental animals; (B) Weekly body weights of mice in each group on a line graph; (C) Final body weights of mice in each group; (D) Body weight gain of mice in 22 weeks; (E) Liver weights of mice in the 22nd week; (F) Mean daily intake of food; (G) Liver morphology, H.E. staining of the liver, (200×; scale: 100μm; black arrow: steatosis, red arrow: inflammation, blue arrow: ballooning degeneration) and oil-red staining of the liver (100×, scale: 100μm); (H) eWAT weights; (I) Lipid droplet staining area ratio. Significant difference between different letters ($P < 0.5$) (n=3), same below.

3.3 ACTE Regulates HFD-induced Disorder of Dirty Lipid Metabolism in Obese mice

Relative to the ND group, mice in the HFD group exhibited marked increases in serum AST, ALT, TG, and TC levels, alongside elevated hepatic TG, TC, and LDL, while hepatic HDL levels were significantly reduced. However, there were no statistically significant variations observed comparing the ND+ACTE group to the ND group. Both the PC and ACTE treatment groups exhibited significant reductions in obese mice serum AST, ALT, Cr, BUN, TG, and TC, as well as hepatic TG, TC and LDL levels, along with a marked increase in hepatic HDL levels (Fig. 3A-C/S2B). In addition, 50 mg/kg ACTE showed the most significant improvement in body weight gain, liver weight, liver TG, liver TC, and Oil-Red-O lipid droplet area, while increasing the dose to 75 mg/kg did not bring better effects; instead, there was a slight decline, exhibiting a bell-shaped non-monotonic dose-response relationship (Fig. S2C). However, food intake, liver function (ALT, AST), and kidney function (Cr, BUN) in the ACTE-H group mice were not significantly different from

those in the ACTE-M groups, indicating that the decline in efficacy at high doses was not due to toxic damage or differences in food intake.

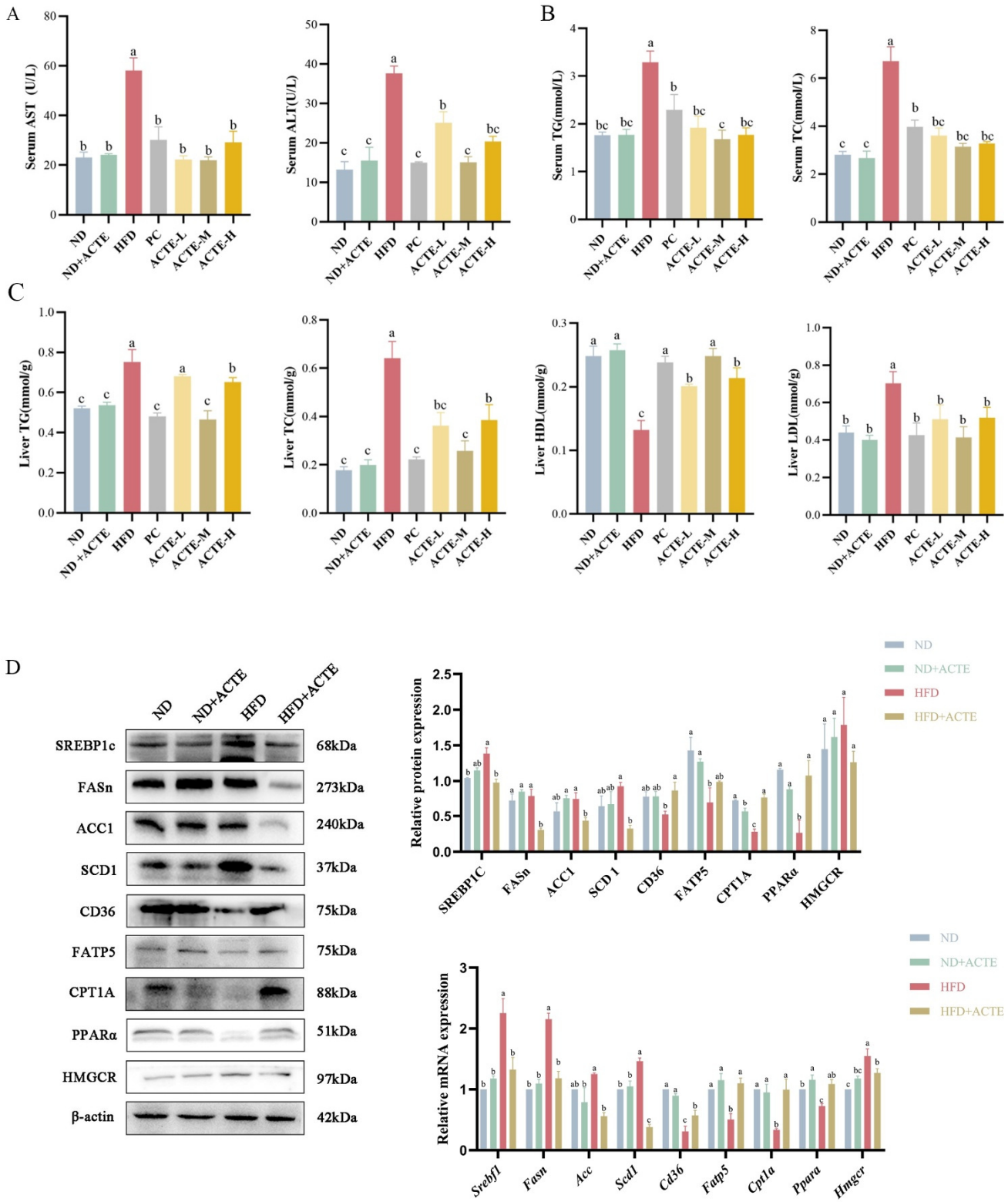

Fig. 3. ACTE modulation of HFD-induced lipid metabolism disorders in obese mice. (A) Serum AST and ALT content; (B) Serum TG and TC content; (C) Liver TG, TC, HDL and LDL content; (D) Relative expression levels of liver SREBP1c, FASn, ACC1, SCD1, CD36, FATP5, CPT1A, PPARα and HMGCR proteins and mRNAs.

Subsequently, we examined lipid synthesis and decomposition-related genes in the liver of normal and obese mice treated with medium-dose ACTE. The HFD group showed a marked reduction in the expression of mRNAs and proteins associated with lipid catabolism (PPARα, CPT1A) and transport (CD36, FATP5)

relative to the ND group, while the expression of adipogenesis-related mRNAs/proteins (SREBP1c, FASn, SCD1) and the mRNA levels of *Hmgcr*, which regulates cholesterol synthesis, were significantly upregulated. As expected, ACTE administration reversed the relative expression levels of these mRNAs and proteins (Fig. 3D). Statistical analysis revealed no notable difference between the ND + ACTE and ND groups. These results suggest that ACTE inhibits HFD-induced hepatic fat accumulation by modulating the expression of lipid metabolism-related mRNAs and proteins.

3.4 Analys the mechanism of action of ACTE by proteomics

We employed HPLC-MS to examine the proteomic composition in the liver. Among the 3,340 identified proteins, the number of differentially expressed proteins between groups is shown in Fig. 4A and depicted as a volcano diagram (Fig. 4B). The top five significant protein fold ratios among the groups are shown in Table S5. Notably, the rate-limiting enzyme CYP7A1, which regulates BA synthesis in the classical pathway, showed a significant increase in the fold difference (1.651987-fold) and a significant decrease in the fold difference (0.65583-fold) after administration of ACTE, in comparison with the ND group. Hierarchical clustering algorithm was used to analyze the differentially expressed proteins (DEP) of each comparison groups by clustering separately, and the data are shown as a heat map (Fig. 4C). the top five DEP fold ratios among the groups are shown in Table S4. By Fisher's exact test method, GO function enrichment analysis was performed on the DEP of each comparison group, and the top five rankings of significance in three categories are shown in Fig. 4D. KEGG pathway enrichment analysis (Fig. 4E) we found that steroid hormone biosynthesis, retinol metabolism was enriched in both comparisons., unsaturated fatty acid biosynthesis, PPAR pathway appeared in the results of both comparisons. Steroid hormones are hydrocorticoids, aldosterone, glucocorticoids, and sex hormones synthesized using CHO as a substrate. Retinoic acid receptor (RAR) and retinoid X receptor (RXR) metabolites activated by retinoids can regulate BA homeostasis by modulating the expression of genes involved in BA metabolism, and also accelerate lipid metabolism by stimulating cholesterol transport. Stearoyl-CoA desaturase (SCD) is involved in the first step of unsaturated fatty acid synthesis, converting the saturated fatty acid palmitic acid to monounsaturated fatty acids. SCD1 expression was memorably upregulated in the HFD group, showing a 5.57-fold increase compared to the ND group. The PPARs pathway regulates several biologically important processes in metabolic disorders, including inflammation, lipids, BA synthesis and glucose metabolism. In addition to this, it is worth noting that there were significant changes in both the primary BA synthesis pathway and bile secretion pathway in the HFD group vs HFD+ACTE group, which was not found in the ND group vs HFD group. This suggests a potential pharmacological effect of ACTE on these pathways. In conclusion, proteomic analysis suggests that the therapeutic effects of ACTE on obesity may be associated with CHO metabolism and BA metabolism.

A

Number of differentially expressed proteins in each comparison group

Comparisons	Down	Up	All
ND vs HFD	38	215	253
HFD vs HFD+ACTE	87	89	176

Comparisons: Comparison group name; Up: Up-regulates the number of differentially expressed proteins; Down: Down-regulates the number of differentially expressed proteins; All: Number of all differentially expressed proteins.

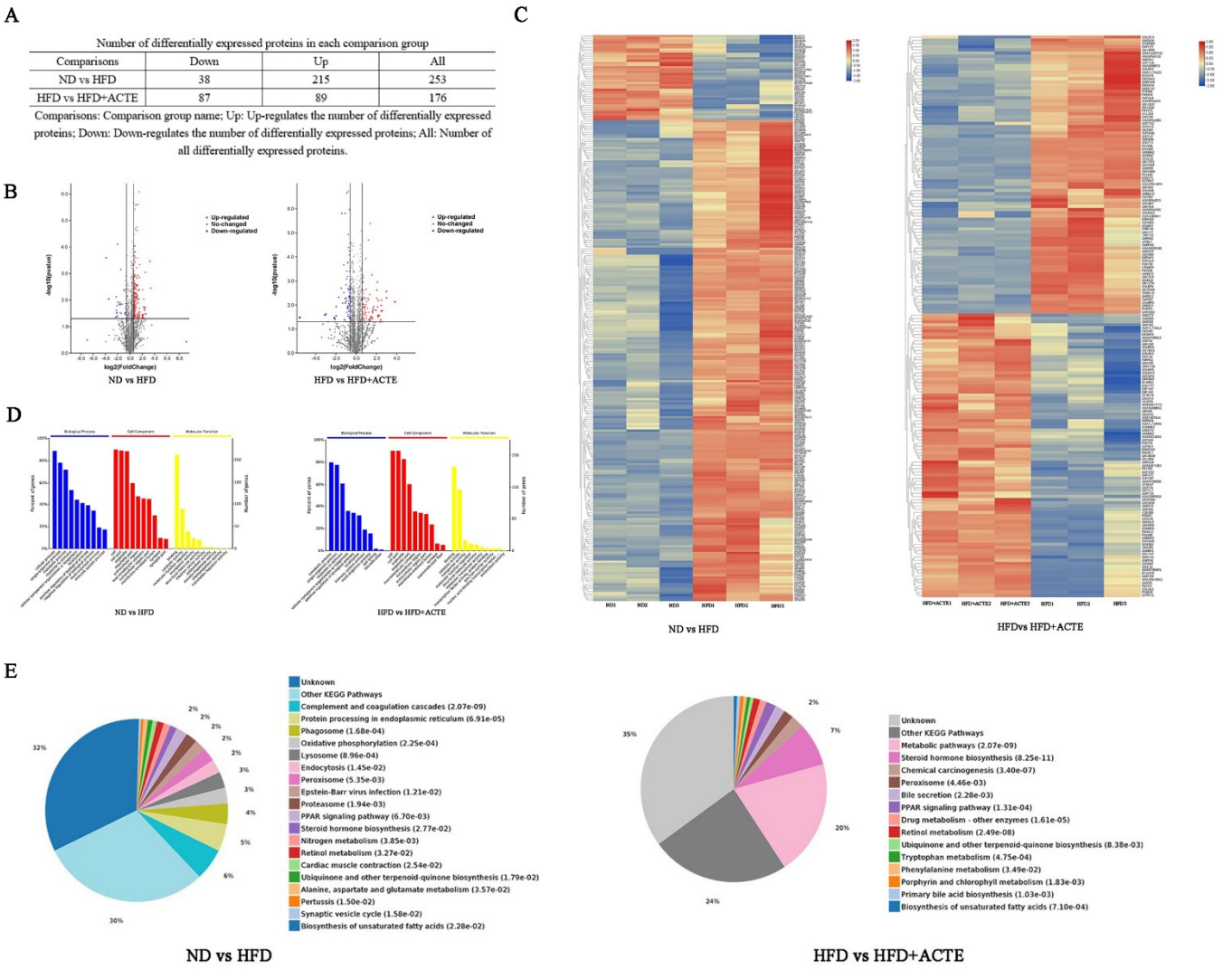

Fig. 4. Liver non-labeled quantitative proteomics assay results. (A) DEP amount in each group; (B) DEP volcano plot, screening DEP by the criterion of multiplicity change of more than 1.5-fold; (C) DEP clustering analysis; (D) GO functional enrichment analysis; (E) KEGG functional enrichment analysis fan plot.

3.5 ACTE regulates HFD-induced disorders of BA metabolism

Based on the common pharmacological effects of ACTE and the results of proteomics assay, we further explored the impact of ACTE on BAs regulation in obese mice. The results showed that long-term HFD resulted in decreased TBA content in liver and ileum epithelial cells and increased TBA content in feces (Fig. 5B). This effect was reversed by ACTE treatment, suggesting that ACTE reduced BAs excretion. To further explore whether ACTE has the potential to modulate BA metabolism, all 21 constituents detected in ACTE were subjected to molecular docking against the endogenous BA receptor FXR. The predicted binding energies and interaction profiles are summarized in Table S6. The results show that 13 active components of ACTE exhibited binding energies all less than or equal to -6.5 (kcal/mol) with FXR. Among them, the four ligands (Paspalinine, Narirutin, Cryptochlorogenic acid and Coumaroylquinic acid) with the lowest binding energies were selected for representative visualization of their optimal binding poses (Fig. 5A).

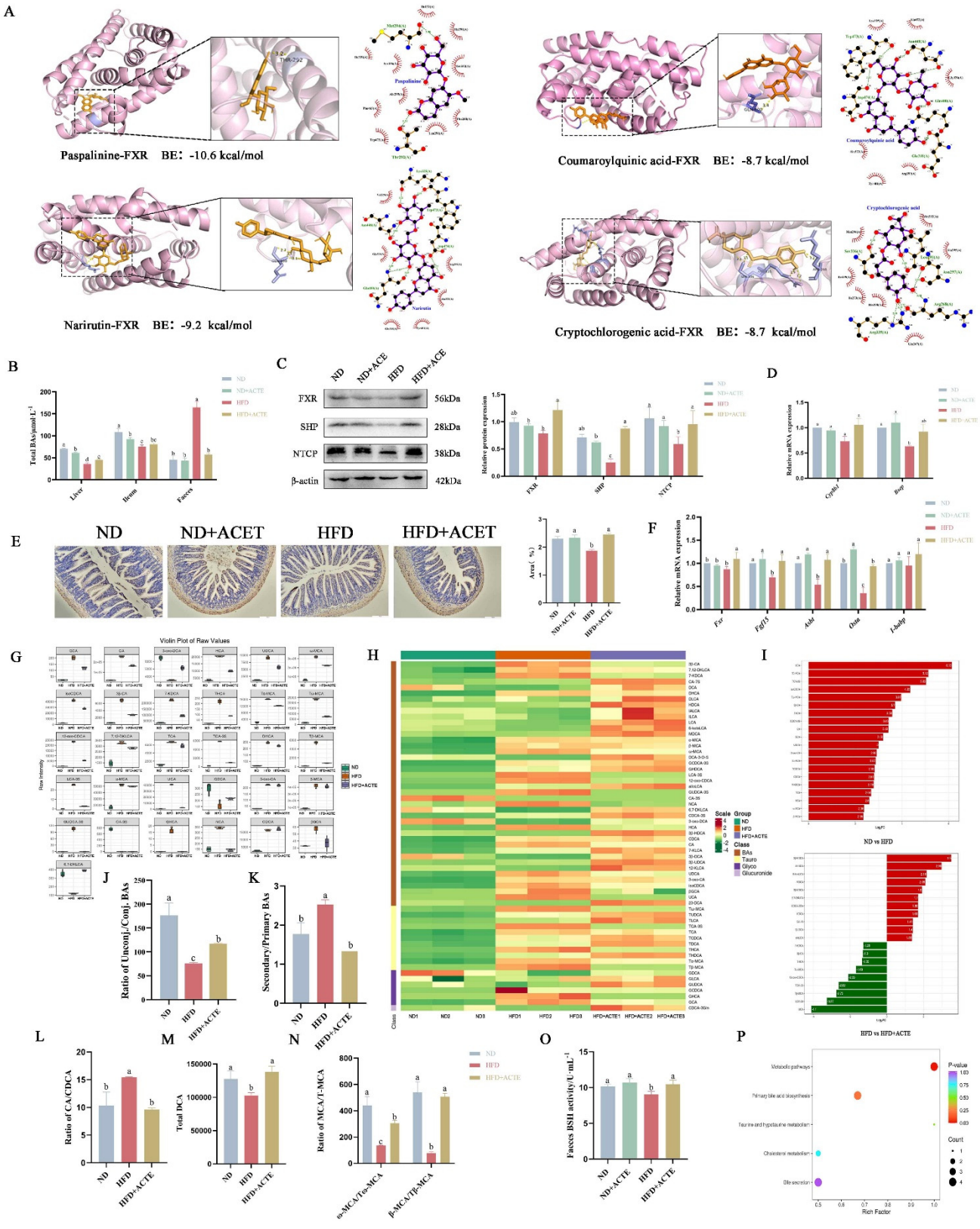

Fig. 5. ACTE regulates HFD-induced BA metabolic disorders. (A) Docking results of ACTE active ingredients and FXR; (B) Total BAs content in liver, ileal epithelial cells and feces; (C) Relative expression levels of hepatic FXR, SHP, and NTCP proteins; (D) Relative expression levels of mRNA for hepatic *Cyp8b1* and *Bsep*; (E) IHC staining of ileal FXR; (F) *Fxr*, *Fgf15*, *Asbt*, *Ostα* and *I-babp* mRNA relative expression levels in ileal epithelial cells; (G) violin plot of differential BAs in mouse cecum contents; (H) differential BA clustering heat map; (I) differential metabolite fold analysis plot; (J) ratio of unconj. versus conj. BAs; (K) ratio of primary versus secondary BAs; (L) ratio of CD versus CDCA; (M) total DCA content; (N) ratio of MCA to TMCA; (O) fecal BSH expression level; (P) differential metabolite KEGG enrichment analysis.

The BAs synthesis and metabolism pathway analysis (Fig. 5C/D) revealed a significant reduction in the protein levels of FXR, SHP, and NTCP, as well as in *Bsep* mRNA expression, which regulates BA entry into the gallbladder, in the livers of the HFD group. This trend was reversed upon the administration of ACTE. A noteworthy reduction in FXR expression was detected in the ileal epithelial cells of the HFD+ACTE group relative to the HFD group. As shown in Fig. 5F, the mRNA levels of *Fxr*, *Fgf15*, *Asbt* and *Ostα* in the ileal epithelial cells of mice in the HFD group were decreased, while ACTE treatment significantly upregulated their expression. The data indicate that ACTE potentially triggers FXR pathway activation in the liver and ileal epithelium of obese mice, thereby promoting BA synthesis and enhancing BA transport and absorption. It is important to highlight that the ND+ACTE group showed significantly lower expression of FXR and SHP proteins in the liver, along with a significant increase in *Osta* mRNA levels in the ileum, relative to the ND group. Simultaneously, a marked decline in hepatic and ileal BA content was observed, implying that ACTE promotes BA flux in healthy mice and facilitates lipid metabolism. Since FXR activity is influenced by the species of BAs, we utilized the LC-MS/MS method to qualitatively and quantitatively detect BAs in the contents of mouse cecum. A total of 65 BAs were detected, with their species and corresponding standard curves listed in Table S7. The ND group exhibited elevated levels of 36 BAs and reduced levels of 5 BAs when compared to the HFD group. In addition, compared to the HFD group, 15 BA counts were elevated and 13 BA counts were decreased in the HFD+ACTE group. Differential BA violin plots, cluster analysis heatmaps and differential multiplicity bar graphs showed that (Fig. 5G-I), ACTE significantly reverses the HFD-induced abnormal elevation of multiple BA levels. Among them, the levels of UCA, 3β-CA, CA, CDCA, β-MCA, ω-MCA, UDCA, HCA, and their coupled BAs, Tω-MCA, Tβ-MCA, TCA-3S, THCA, TCDCA, GCA, and GUDCA were markedly higher in the HFD group than in the ND group, whereas the administration of A. capillaris Thunb. could significantly down-regulate the contents of UCA, CA, HCA, GHCA, GUDCA-3s, 3β-CA, Tω-MCA, Tβ-MCA, TCA-3S, LCA -3S, THCA and Tα-MCA, etc. As shown in Fig. 5J, ACTE administration elevated the ratio of unconj. BAs to conj. BAs compared to the HFD group. Notably, the ratios of β-MCA/Tβ-MCA and ω-MCA/Tω-MCA were significantly elevated (Fig. 5N), which may be attributed to the elevated BSH content in the feces (Fig. 5O). Moreover, Tβ-MCA, Tω-MCA and THCA were significantly and positively correlated with body weight and serum TG, TC levels in mice (Fig. S3C). Additionally, we found that administration of ACTE increased the percentage of primary BAs in the cecum contents (Fig. 5K), and significantly reduced the CA/CDCA ratio (Fig. 5L),Notably the level of total DCA was also significantly higher(Fig. 5M). The differential metabolite KEGG pathway (Fig. 5P) was enriched in the pathways of CHO metabolism, BA secretion, taurine and hypotaurine metabolism, primary BAs biosynthesis, and metabolic pathways. These findings indicate that ACTE modifies the BA composition in cecal contents and reduces the proportion of un conj. BAs, potentially linked to elevated intestinal BSH levels.

3.6 ACTE Improves Ecological Dysbiosis of Gut Microbiota

The gut microbiota is essential for regulating BA homeostasis in the host. To evaluate the effects of ACTE on microbial communities, 16S rRNA gene sequencing and subsequent bioinformatics analysis were conducted on cecal contents from mice. The HFD group exhibited notably lower levels in multiple diversity indices—Chao1, Shannon, Pielou's evenness, Simpson, observed species, and Faith's PD—compared to the ND group, indicating that extended HFD feeding impairs gut microbial richness, genetic variation, and ecological balance (Fig. 6A). However, the microbial richness and diversity of the mouse cecum were enormously restored following ACTE treatment. Principal component analysis (PCA)-based β-diversity analysis revealed clear separation among the three groups (Fig. 6B). These results suggest that ACTE supplementation ameliorates ecological dysregulation of the gut microbiota in HFD mice. The Venn diagram (Fig. 6C) revealed distinct OTU counts in each group—1,277 in ND, 320 in HFD, and 729 in HFD+ACTE—highlighting substantial differences in intestinal microbiota composition across the groups.

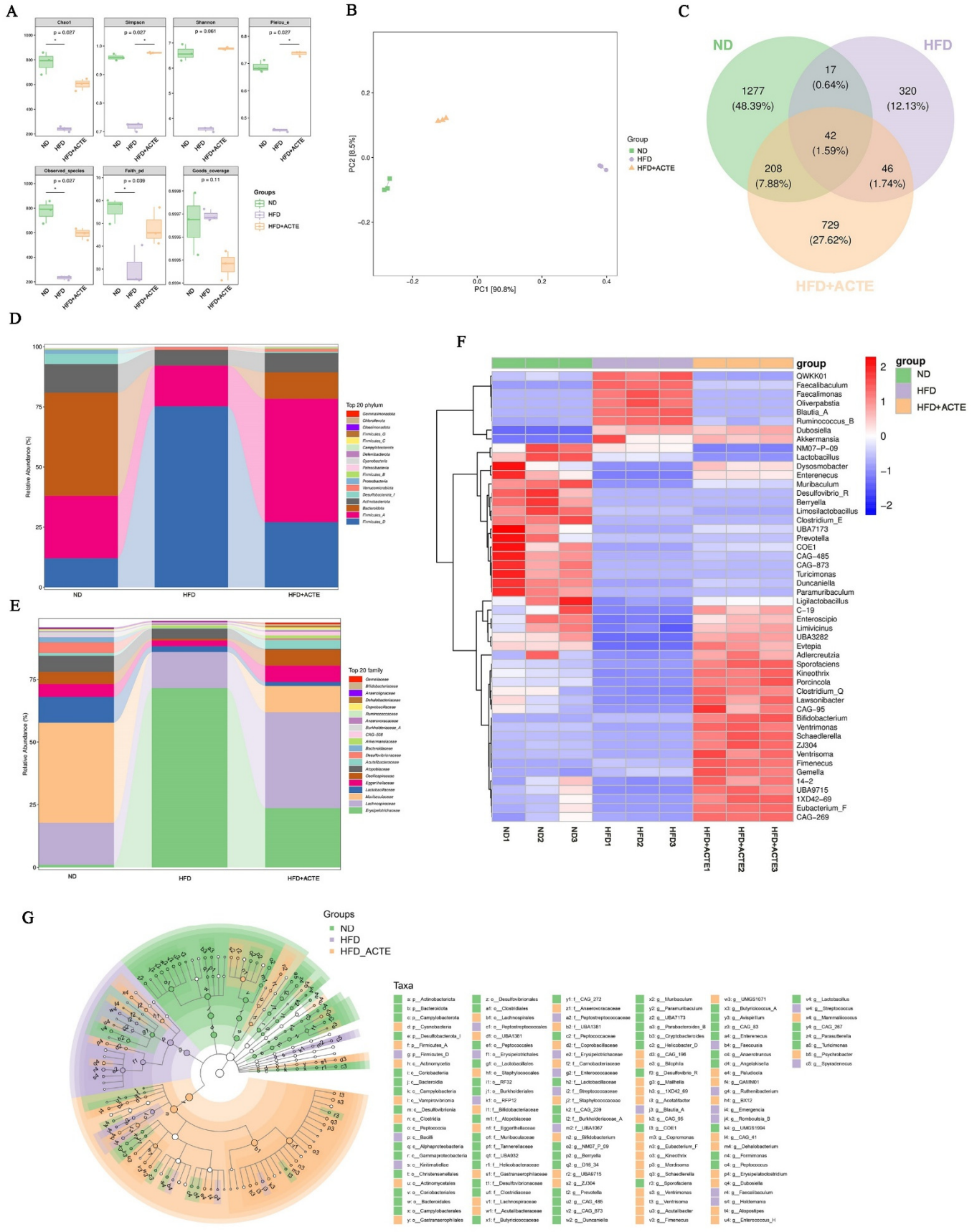

Fig. 6. Effect of ACTE on gut microbiota and intestinal mucosal barrier in Obese mice. (A) α-diversity indices; (B) PCA based on β-diversity; (C) Venn diagram of OTU distribution; (D) Phylum-level compositional analysis of the gut microbiota; (E) Family-level compositional analysis of the gut microbiota; (F) Heatmap of gut microbiota composition across different groups; (G): Classification units for intergroup differences based on classification hierarchy trees.

Compositional analyses at the phylum level revealed (Fig. 6D) that, mice in the HFD group had a significantly higher relative abundance of *Firmicutes*, and significantly lower *Bacteroidetes*, *Actinobacteriota*, *Desulfobacterota*, and *Proteobacteria*. Conversely, the HFD+ACTE group exhibited an opposite pattern relative to the HFD group. The family level showed (Fig. 6E) that, compared to the ND group, mice in the HFD group had a significantly lower abundance of *Bifidobacteriaceae*, *Lactobacillacene*, and observably higher abundance of *Erysipelotrichaceae*. The relative abundance of *Bifidobacteriaceae* and *Lachnospiraceae* was elevated and *Erysipelotrichaceae* was significantly reduced in the HFD+ACTE group compared to the HFD mice. Analysis of the interaction heatmap of the species composition of the intestinal flora in each group (Fig. 6F) showed that the relative abundance of *Faecalibaculum*, *Ruminococcus-B*, *Blautia-A*, *Faecalimonas*, and *Oliverpabstia* was higher in the HFD mice than in the rest of the groups, and *Limivicinus*, *Evtepia*, *Enterenecus* and *Dysosmobacter* had significantly lower relative abundance. Particularly, the opposite was true for the ACTE group. In the LEfSe (linear discriminant analysis of effect size) analysis (Fig. 6G), *Lactobacillus* spp. were found to be most abundant in the ND group. *Bifidobacterium* spp. and the *Lachnospiraceae* family were significantly enriched in the ACTE group, suggesting that the intervention may have facilitated the colonization and propagation of beneficial bacteria. In contrast, the HFD group was significantly enriched in the *Firmicutes_D* phylum, the *Erysipelotrichaceae* family, and *Faecalibaculum* spp., which have been suggested to be associated with metabolic disorders and intestinal inflammation in previous studies. The histogram of abundance between groups revealed that the relative abundance of *Bifidobacterium* and *Lachnospiraceae* was even significantly higher than that of the ND group (Fig. S3A). Analysis of the species composition of differential MetaCyc metabolic pathways revealed that most of the genera in the HFD group were largely uninvolved in the metabolic functions related to taurine dissociation and fatty acid β-oxidation, whereas the contribution of the ACTE group was significantly enhanced in both pathways, especially with the *Lachnospiraceae* family (unclassified) as the major contributing group (Fig. S3B). Spearman correlation analysis revealed that Lachnospiracea spp. was significantly negatively correlated with serum TG; *Lachnospiracea* spp. and *Bifidobacterium* spp. are significantly and positively correlated with FXR activity, LCA and BSH content (Fig. S3C). Taken together, the ACTE intervention effectively enhanced the abundance of *Bifidobacteria* and *Lachnospiraceae*, inhibited the HFD-induced expansion of harmful flora, and demonstrated a positive role in remodeling the structure of the intestinal flora and regulating host metabolism.

3.7 Effects of ACTE on the Gut Barrier and Hepatic Nf-κB Pathway and NLRP3 Pathway

The ileal H.E. results showed (Fig. 7A) that the ratio of villus height to crypt depth was significantly lower in the HFD group, and ACTE administration increased the ratio. The WB data (Fig. 7B) indicated a remarkable decrease in ZO-1 and Claudin-1 protein levels in the HFD group compared to the ND group. This change was reversed with ACTE treatment, indicating that HFD could lead to a decrease in the tight junction of ileal tissues and damage to the intestinal mucosa and ACTE administration could alleviate gut barrier impairment. Damage to the intestinal barrier facilitates the entry of substantial quantities of LPS into the

bloodstream. Therefore, we further detected the level of LPS in the bloodstream, which showed (Fig. 7C) that compared with the normal mice, the level of LPS in the serum of the HFD group was elevated; the level of LPS was reduced by the administration of ACTE. Meanwhile ileal epithelial cell WB and PCR results showed (Fig. 7D/E) that inflammatory factors IL-1β, IL-6, and TNF-α were increased in the HFD group, but these levels decreased after ACTE administration. These results indicate that ACTE administration enhanced the intestinal barrier and reduced the expression of serum LPS and ileal inflammatory factors in Obese mice.

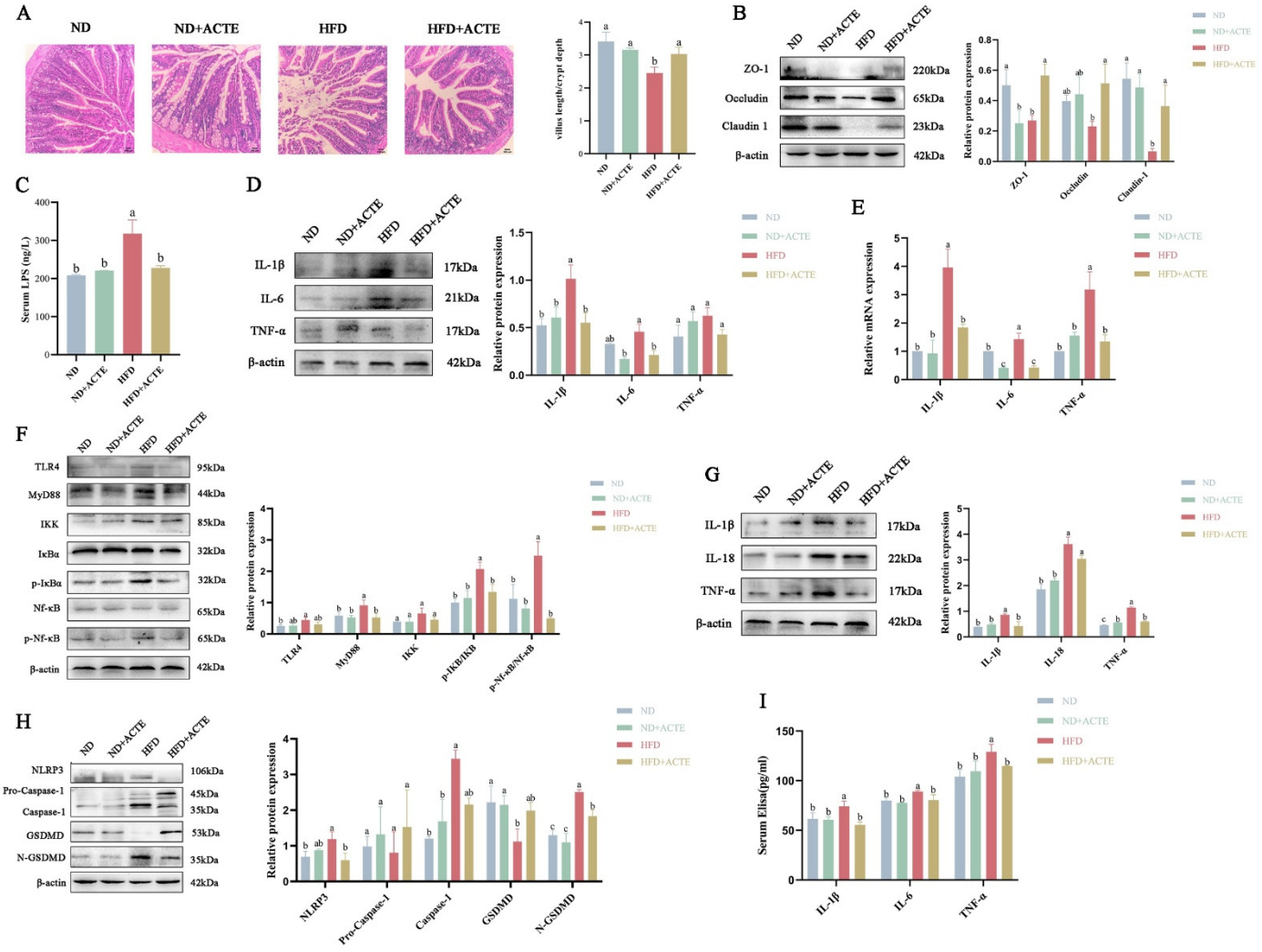

Fig. 7. Effect of ACTE on the ileal barrier and hepatic Nf-κB/NLRP3 pathway. (A) Ileal H.E. staining (200×, scale: 100μm) and ileal intestinal villus length/crypt depth; (B) Relative expression levels of ileal ZO-1, Occludin, Claudin-1 proteins; (C) Serum LPS content; (D) Relative expression levels of ileal IL-1β, IL-6, and TNF-α proteins; (E) Relative expression of ileal IL-1β, IL-6, and TNF-α mRNA; (F) Relative expression levels of hepatic TLR4, MyD88, IKK, IKBα/p-IKBα, and Nf-κB/p-Nf-κB proteins; (G) Relative expression levels of hepatic IL-1β, IL-18, and TNF-α proteins; (H) Relative expression levels of hepatic NLRP3, Pro-Caspase-1, Caspase-1, GSDMD, and N- GSDMD proteins; (I) Hepatic inflammatory factors IL-1β, IL-6, TNF-α relative expression levels.

LPS can bind to TLR4, triggering the NF-κB pathway and resulting in the increased release of pro-inflammatory mediators. The WB results (Fig. 7F) demonstrated higher levels of TLR4, MyD88, IKK, p-IκBα/IκBα and p-NF-κB/NF-κB proteins in the HFD group. ACTE suppresses phosphorylation of Nf-κB, IκB and overexpression of MyD88. This suggests that ACTE could exert anti-inflammatory effects through the Nf-κB pathway. As seen in Fig. 7G/I, long-term high-fat diet intake markedly elevated hepatic protein

levels of TNF-α, IL-1β, and IL-6, whereas administration of ACTE down-regulated their expression. Referring to Fig. 7H, HFD notably upregulated NLRP3, Caspase-1, and N-GSDMD protein expression levels, while downregulating GSDMD expression. Moreover, ACTE administration markedly suppressed the expression of these proteins. In comparison to the ND group, no significant alterations were observed in the ND+ACTE group, indicating that the medium dose of ACTE did not contribute to inflammation or pyroptosis. The findings indicate that long-term HFD feeding causes liver injury in mice, stimulates NF-κB activation, and promotes cleavage of NLRP3 and GSDMD in the liver. ACTE administration inhibits not only NLRP3 but also Nf-κB pathways, reduces the release of inflammatory factors, and alleviates hepatocellular injury in Obese mice.

4. Discussion

In recent years, the focus on targeting the BA metabolic pathway has emerged as a novel research direction for the treatment of obesity. Although FXR agonists, such as UDCA and OCA, have already been employed in clinical practice, their associated adverse effects, including skin irritation, fatigue, and gastrointestinal discomfort, have limited their clinical application [18, 19]. A. capillaris Thunb., a plant commonly dried and brewed into ACTE, exhibits cholagogic, anti-inflammatory, sterilizing, and blood pressure-lowering properties. The main chemical constituents of ACTE that detected in this study were organic acids, coumarins, flavonoids, coumaric acid, and volatile oils. In the dose- response study, we observed that the ACTE-M group (50 mg/kg) exhibited the best therapeutic effect on obesity model mice, after the dose increase, a bell-shaped dose-response relationship was observed, consistent with the non-monotonic pharmacodynamic model described in the literature. We then explored the mechanism through which ACTE-M in medium doses improves obesity through the gut-liver axis. Our results provide new insights and a conceptual foundation for utilizing dietary approaches in the prevention of obesity.

SREBP1c regulates the de novo synthesis of FFA and promotes their esterification and desaturation by modulating downstream factors such as FASN, ACC1 and SCD1 [20]. PPARα, when activated, stimulates the expression of CD36, FATP5 and CPT1A, increases the transmembrane transport of long-chain FFAs and β-oxidation of FFAs, contributing to the reduction of hepatic TG content [21, 22]. HMGCR is a critical enzyme in the CHO biosynthetic pathway in hepatocytes, driving the conversion of mevalonate [22]. Our research demonstrated that ACTE treatment led to a significant reduction in the expression of SREBP1c and its downstream targets (FASN, ACC1, SCD1), as well as HMGCR in obese mouse livers. Conversely, the expression levels of PPARα, CD36, and CPT1A were significantly increased, while serum and liver contents of TG, TC, and LDL were observably reduced. The data imply that ACTE inhibits endogenous FAs and CHO synthesis, accelerate the transport and oxidative decomposition of FAs, and mitigates hepatic fat buildup, aligning with Liang's observations [16].

Diseases of lipid metabolism are often caused by abnormal BA metabolism. Xu and Cui showed that Yinchenhao decoction alleviated HFD-induced obesity by increasing FXR and APOA1 expression [23]. Active components detected in ACTE, such as chlorogenic acid, promote lipid metabolism balance by regulating the

AMPK/FXR/SREPB-1c signaling pathway [24]. Dietary isoquercetin and isorhamnetin significantly modulate crosstalk between BA and specific gut bacteria in NAFLD mice via FXR, reducing lipid deposition [25, 26].Our results suggest that administration of ACTE promotes the expression of hepatic FXR/SHP and ileal epithelial cell FXR/FGF15, while reducing the expression of the SREBP1c pathway. CYP7A1 catalyze the conversion of CHO into the primary BA- CA in the liver [27, 28]. Meanwhile CYP8B1 is essential for transforming the primary BA-CDCA, produced via the alternative pathway back into CA. The conversion of CHO to BAs is regulated by a negative feedback loop through the FXR-SHP pathway, which controls CYP7A1 transcription [29]. Increased BAs depletes hepatic CHO stores, which in turn increases hepatic LDL receptor expression, promoting increased uptake of CHO from the internal circulation [30]. Our findings indicate that activation of FXR in obese mice by ACTE inhibits the overexpression of CYP7A1, decreases the CA/CDCA ratio, and limits excessive BAs, ultimately decreasing serum TC levels.

The intestines and the liver exchange substances via somatic circulation - the bidirectional interaction known as gut-liver axis. The transport of BAs between the intestines and liver is referred to as the enterohepatic circulation. When activated by BAs, FXR binds to inverted repeat sequence 1 (IR-1) to promote the expression of BSEP, a rate-limiting transporter in the enterohepatic circulation of BAs [31]. Clinical observations in MASH patients revealed downregulation of both BSEP and NTCP expression. These results are in agreement with our previous observations. mRNA expression levels of *Asbt*, *I-babp*, and *Ostα* were up-regulated in ileal epithelial cells, which suggests that ACTE promotes the reabsorption of BAs in the intestinal tract and reduces the BAs exocytosis, which corresponds to the results of TBA content in the feces. Clifford et al. reported that treatment with dietary supplementation with the FXR agonist (GSK2324) reduced BAs and led to decreased lipid absorption in obese mice [19]. Based on the molecular docking results and cell model validation, we hypothesized that the active ingredients contained in ACTE activate FXR, promote BAs transport and reabsorption, and reduce BAs levels in the small intestine, thereby reducing lipid absorption. Interestingly, ACTE can increase BA flow in healthy mice, which is conducive to the digestion and absorption of lipids, indicating that ACTE can dynamically regulate BA metabolism.

BAs are not only involved in the regulation of lipid metabolism and cholesterol homeostasis, but are also endogenous ligands for FXR [32]. We found that ACTE intervention significantly reversed the HFD-induced disruption of the constitutive feature composition of BAs and reduced the levels of FXR antagonists such as THCA (-1.35-fold), Tω-MCA (-1.68-fold), and Tβ-MCA (-2.75-fold). At the same time, ACTE significantly elevated the levels of the secondary BAs DCA, LCA, HDCA and their derivatives, which as TGR5 receptor agonists, have been shown to promote lipolysis and GLP-1 secretion and enhance white adipose tissue thermogenesis [33-35]. HDCA supplementation can treat MASLD by inhibiting nucleoplasmic shuttling in PPARα cells [36]. In an antibiotic-induced obese mouse model of gut microbiota disruption, Tβ-MCA accumulation and decreased DCA and LCA levels were observed [37]. Chao et al. [38] showed that the impaired de-conjugation capacity of the intestinal flora of MASLD model mice resulted in a reduced ratio of unconj. BAs, which hindered the reabsorption of BAs. These studies indicate that, in the obese state, gut microbiota

disruption inhibits conj. dissociation and reduces the conversion of primary BAs to secondary BAs. ACTE treatment notably boosted the fecal BSH activity, which in turn facilitated the unconj. of BAs. Notably, the ω-MCA/Tω-MCA and β-MCA/Tβ-MCA ratios were significantly elevated. Taken together, these results suggest that ACTE can also regulate the BAs hepatic and intestinal circulation by improving intestinal flora, promoting the unconj. of FXR antagonists (e.g., THCA, Tβ-MCA and Tω-MCA), and enhancing the conversion of secondary BAs (e.g., DCA and LCA), thereby promoting the activation of the FXR signaling pathway.

The gut microbiota is intimately linked to obesity development. Patients with MASLD are commonly characterized by decreased intestinal microbial diversity, disorganized flora structure, and impaired intestinal barrier function [39]. HFD significantly attenuated the alpha diversity of the intestinal flora (decrease in Shannon and Chao1 indices), whereas the ACTE intervention significantly improved the diversity and abundance of the flora, contributing to the restoration of microecological balance. Approximately 90% of the gut microbial composition in humans and mice consists of *Firmicutes* and *Bacteroidete* [40, 41]. An increased ratio of *Firmicutes* to *Bacteroidetes* (F/B) has been observed in both obese mice and humans, which is associated with the efficiency of energy uptake in patients, leading to increased energy absorption and fat storage [42]. ACTE treatment was found to reduce the relative abundance of *Firmicutes* and increases the abundance of *Bacteroidetes*, which in turn reduces the F/B ratio.

Supplementing with probiotics or prebiotics enhances the self-regulation of the intestinal microbiota [43]. It was found that chlorogenic acid, the active ingredient in ACTE, reversed the HFD-induced intestinal dysbiosis and promoted the growth of *Bacteroides* and *Lactobacillaceae* [44]. We found that ACTE intervention notably enhanced the proportion of beneficial bacteria, including *Bifidobacterium*, *Lachnospiraceae*, *Ligilactobacillus*, *Bacteroides,* etc. The abundance of *Bifidobacterium* and *Lachnospiraceae* was even higher than that of the ND group. Zhang et al. found that *Bifidobacterium* spp. and *Bacteroides* spp. were depleted in high-fat/high-cholesterol (HFHC)-fed mice [45]. Wang et al. demonstrated that supplementation of HFD mice with *Bifidobacterium* spp. reduced hepatic TG, TC content [46]. *Lachnospiracease* spp. and *Ligilactobacillus* spp. are potentially beneficial bacteria involved in the metabolism of carbohydrates, the production of secondary BAs, the regulation of glucose-lipid levels, and the enhancement of the efficiency of energy utilization to provide energy to the host [47, 48]. The results of the present study showed that ACTE intervention induced *Lachnospiraceae* to participate in taurine degradation and fatty acid β-oxidation, which in turn increased BSH levels, activated FXR signaling. Subsequently, we should conduct fecal microbiota transplantation (FMT) or single-bacterial transplantation experiments to further verify the causal effect of gut microbiota on FXR activation. In addition, the ACTE intervention significantly reduced the relative abundance of certain conditionally pathogenic bacteria, such as *Faecalibaculum*, *Ruminoccoccus-B*, and *Erysipelotrichaceae*, etc. Over-representation of *Ruminoccoccoccus-B* and *Faecalibaculum* has been linked to irritable bowel syndrome characterized by diarrhea and its abundance was positively correlated with the malignant obesity index score [49, 50]. Xu et al.

found an increase in *Faecalibaculum* and *Ruminococcaceae UCG-010* following the transplantation of fecal microbiota from dyslipidemic donors into mice [51, 52]. Enrichment of *Erysipelotrichaceae* was associated with intestinal inflammation and elevated risk of colorectal cancer [53]. In this research, we found that the relative prevalence of all the aforementioned conditionally pathogenic bacteria was notably decreased in mice treated with ACTE in comparison to those fed HFD. In summary, ACTE significantly increased the relative abundance of *Bifidobacterium* and *Lachnospiraceae*, restored the balance between beneficial and conditionally pathogenic gut bacteria, thereby reshaping the intestinal microecological structure and improving the host metabolic status.

Beneficial bacteria can inhibit the growth of pathogenic microorganisms through competitive exclusion and production of antimicrobial substances, which together with the tight junction complexes (e.g., ZO-1 and occludin) in the intestinal epithelial cells constitute the intestinal mechanical barrier. When the intestinal barrier function is impaired, harmful microorganisms as well as abnormal metabolites migrate through the portal vein, thereby triggering an inflammatory response [54]. Specifically, LPS promotes IκB kinase phosphorylation through activation of the TLR4/MyD88 complex, which in turn leads to the depolymerization and translocation of Nf-κB into the nucleus and promotes the release of pro-inflammatory factors, such as IL-6/TNF-α [55, 56]. ACTE has demonstrated its ability to reduce inflammatory responses triggered by LPS by inhibiting the activation of Nf-κB in both rat liver and HepG2 cells [57].We found that ACTE intervention significantly upregulated the expression of ZO-1 and occludin, reduced serum LPS levels, inhibited the activation of the hepatic Nf-κB pathway, attenuated hepatic inflammation, and alleviated obesity-related injury. In addition, it was shown that quinic acid and scopolin, the main active ingredients in ACTE, increased the abundance of beneficial genera such as *Bifidobacterium spp*. and decreased the abundance of harmful genera such as *Shigella spp*., Maintained the intestinal barrier and inhibited the MyD88/NF-κB signaling pathway. Notably, the effect of quinic acid on intestinal inflammation was attenuated after antibiotic treatment. This further supports the mechanism by which ACTE ameliorates the inflammatory response through gut flora regulation [58, 59].

Activation of Nf-κB is a precondition for the formation of NLRP3 inflammatory vesicles, which in turn recruits and activates the caspase-1 precursor, which can activate IL-1β and IL-18. Simultaneously, GSDMD generates an N-terminal fragment capable of forming pores in the cell membrane, ultimately resulting in cell swelling and lysis, amplifying the inflammatory response [60]. ACTE inhibits NLRP3-mediated cellular pyroptosis and prevents inflammatory bursts. In addition to the activation of NLRP3 by the inflammatory response triggered by the intestinal microbiota, FXR can negatively regulate via feedback NLRP3 inflammatory vesicles [61]. Studies have shown that hepatic fat content is decreased in GSDMD knockout mice. In this group of mice, PPARα, which plays a pivotal role in fat breakdown, was significantly overexpressed, while SREBP1c, responsible for stimulating lipogenesis, showed reduced expression [62], suggesting a potential interaction within the FXR-NLRP3-SREBP1c pathway in maintaining maetabolic homeostasis. However, this hypothesis requires further investigation.

5. Conclusion

In summary, ACTE alleviated obesity-associated hepatic steatosis and inflammatory responses, with the mid dose exhibiting the greatest efficacy. Mechanistically, ACTE can reduce hepatocyte inflammatory response and focal necrotic injury by altering the gut microbial composition, enhancing the intestinal barrier, lowering the serum level of LPS, and increasing BSH activity, altering the composition of BAs, thus activating the FXR pathway; In parallel, multiple absorbable active constituents within ACTE are capable of directly engaging FXR, further promoting enterohepatic circulation of bile acids and improving obesity-related metabolic abnormalities. However, this study still has certain limitations. Further validation through FMT, single-compound verification, and subsequent clinical research is needed to conclusively confirm the therapeutic efficacy and mechanism of action of ACTE in humans.

Consent for publication

Permission to publish this article has been obtained from all experimental participants, and copies of the consent form can be viewed at any stage.

Data availability statement

The data that support the findings of this study are openly available in Mendeley Data at http://data.mendeley.com, reference number DOI: 10.17632/jkj5fzhstj.1

References

[1] M. Benedict, X. Zhang, Non-alcoholic fatty liver disease: An expanded review, World J Hepatol. 9 (2017) 715-732. https://doi.org/10.4254/wjh.v9.i16.715.

[2] Y.Y. Chen, M.M. Yeh, Non-alcoholic fatty liver disease: A review with clinical and pathological correlation, J Formos Med Assoc. 120 (2021) 68-77. https://doi.org/10.1016/j.jfma.2020.07.006.

[3] C.J. Liou, Y.W. Dai, C.L. Wang, et al., Maslinic acid protects against obesity-induced nonalcoholic fatty liver disease in mice through regulation of the Sirt1/AMPK signaling pathway, FASEB J. 33 (2019) 11791-11803. https://doi.org/10.1096/fj.201900413RRR.

[4] C.D. Hansen, E.M. Gram-Kampmann, J.K. Hansen, et al., Effect of Calorie-Unrestricted Low-Carbohydrate, High-Fat Diet Versus High-Carbohydrate, Low-Fat Diet on Type 2 Diabetes and Nonalcoholic Fatty Liver Disease : A Randomized Controlled Trial, Ann Intern Med. 176 (2023) 10-21. https://doi.org/10.7326/m22-1787.

[5] B.C. Ferslew, G. Xie, C.K. Johnston, et al., Altered Bile Acid Metabolome in Patients with Nonalcoholic Steatohepatitis, Dig Dis Sci. 60 (2015) 3318-3328. https://doi.org/10.1007/s10620-015-3776-8.

[6] J.Y. Chiang, Bile acids: regulation of synthesis, J Lipid Res. 50 (2009) 1955-1966. https://doi.org/10.1194/jlr.R900010-JLR200.

[7] N. Méndez-Sánchez, C.E. Coronel-Castillo, A.L. Ordoñez-Vázquez, Current Therapies for Cholestatic Diseases, Biomedicines. 11 (2023) https://doi.org/10.3390/biomedicines11061713.

[8] P.P. Chothe, L.C. Czuba, E.N. Ayewoh, et al., Tyrosine Phosphorylation Regulates Plasma Membrane Expression and Stability of the Human Bile Acid Transporter ASBT (SLC10A2), Mol Pharm. 16 (2019) 3569-3576. https://doi.org/10.1021/acs.molpharmaceut.9b00426.

[9] J.H. Park, M. Iwamoto, J.H. Yun, et al., Structural insights into the HBV receptor and bile acid transporter NTCP, Nature. 606 (2022) 1027-1031. https://doi.org/10.1038/s41586-022-04857-0.

[10] R.F. Kunst, H.J. Verkade, R.P.J. Oude Elferink, et al., Targeting the Four Pillars of Enterohepatic Bile Salt Cycling; Lessons From Genetics and Pharmacology, Hepatology. 73 (2021) 2577-2585. https://doi.org/10.1002/hep.31651.

[11] M.H. Mohamad Nor, N. Ayob, N.M. Mokhtar, et al., The Effect of Probiotics (MCP(®) BCMC(®) Strains) on Hepatic Steatosis, Small Intestinal Mucosal Immune Function, and Intestinal Barrier in Patients with Non-Alcoholic Fatty Liver Disease, Nutrients. 13 (2021) https://doi.org/10.3390/nu13093192.

[12] S.N. Chen, Y. Tan, X.C. Xiao, et al., Deletion of TLR4 attenuates lipopolysaccharide-induced acute liver injury by inhibiting inflammation and apoptosis, Acta Pharmacol Sin. 42 (2021) 1610-1619. https://doi.org/10.1038/s41401-020-00597-x.

[13] H.-Y. Hung, S.-C. Kuo, Recent Studies and Progression of Yin Chen Hao (茵陳蒿 Yīn Chén Hāo), a Long-term Used Traditional Chinese Medicine, Journal of Traditional and Complementary Medicine. 3 (2013) 2-6. https://doi.org/10.4103/2225-4110.106533.

[14] M.H. Yen, C.I. Huang, M.S. Lee, et al., Artemisia capillaris inhibited enterovirus 71-induced cell injury by preventing viral internalization, The Kaohsiung Journal of Medical Sciences. 34 (2017) 150-159. https://doi.org/10.1016/j.kjms.2017.11.005.

[15] H.N. Mu, Q. Zhou, R.Y. Yang, et al., Caffeic acid prevents non-alcoholic fatty liver disease induced by a high-fat diet through gut microbiota modulation in mice, Food Res Int. 143 (2021) 110240. https://doi.org/10.1016/j.foodres.2021.110240.

[16] M. Liang, M. Huo, Y. Guo, et al., Aqueous extract of Artemisia capillaris improves non-alcoholic fatty liver and obesity in mice induced by high-fat diet, Frontiers in Pharmacology. 13 (2022) https://doi.org/10.3389/fphar.2022.1084435.

[17] Y. Dai, Z. Dou, R. Zhou, et al., Quality Evaluation of Artemisia capillaris Thunb. Based on Qualitative Analysis of the HPLC Fingerprint and UFLC-Q-TOF-MS/MS Combined with Quantitative Analysis of Multicomponents, Journal of analytical methods in chemistry. 2021 (2021) 5546446. https://doi.org/10.1155/2021/5546446.

[18] J. Liu, J. Sun, J. Yu, et al., Gut microbiome determines therapeutic effects of OCA on NAFLD by modulating bile acid metabolism, NPJ Biofilms Microbiomes. 9 (2023) 29. https://doi.org/10.1038/s41522-023-00399-z.

[19] B.L. Clifford, L.R. Sedgeman, K.J. Williams, et al., FXR activation protects against NAFLD via bile-acid-dependent reductions in lipid absorption, Cell Metab. 33 (2021) 1671-1684.e1674. https://doi.org/10.1016/j.cmet.2021.06.012.

[20] S. Ouyang, S. Zhuo, M. Yang, et al., Glycerol Kinase Drives Hepatic de novo Lipogenesis and Triglyceride Synthesis in Nonalcoholic Fatty Liver by Activating SREBP-1c Transcription, Upregulating DGAT1/2 Expression, and Promoting Glycerol Metabolism, Advanced science (Weinheim, Baden-Wurttemberg, Germany). 11 (2024) e2401311. https://doi.org/10.1002/advs.202401311.

[21] N. Bougarne, B. Weyers, S.J. Desmet, et al., Molecular Actions of PPARα in Lipid Metabolism and Inflammation, Endocr Rev. 39 (2018) 760-802. https://doi.org/10.1210/er.2018-00064.

[22] Q. Zhang, X. Kong, H. Yuan, et al., Mangiferin Improved Palmitate-Induced-Insulin Resistance by Promoting Free Fatty Acid Metabolism in HepG2 and C2C12 Cells via PPARα: Mangiferin Improved Insulin Resistance, J Diabetes Res. 2019 (2019) 2052675. https://doi.org/10.1155/2019/2052675.

[23] L. Xu, H. Cui, Yinchenhao Tang alleviates high fat diet induced NAFLD by increasing NR1H4 and APOA1 expression, J Tradit Complement Med. 13 (2023) 325-336. https://doi.org/10.1016/j.jtcme.2023.02.010.

[24] J. Xu, W. Jia, G. Zhang, et al., Extract of Silphium perfoliatum L. improve lipid accumulation in NAFLD mice by regulating AMPK/FXR signaling pathway, J Ethnopharmacol. 327 (2024) 118054. https://doi.org/10.1016/j.jep.2024.118054.

[25] C. Zhang, Z. Shi, H. Lei, et al., Dietary Isoquercetin Reduces Hepatic Cholesterol and Triglyceride in NAFLD Mice by Modulating Bile Acid Metabolism via Intestinal FXR-FGF15 Signaling, J Agric Food Chem. 71 (2023) 7723-7733. https://doi.org/10.1021/acs.jafc.3c00952.

[26] X. La, Z. Zhang, C. Dong, et al., Isorhamnetin in Quinoa Whole-Grain Flavonoids Intervenes in Non-Alcoholic Fatty Liver Disease by Modulating Bile Acid Metabolism through Regulation of FXR Expression, Foods. 13 (2024) https://doi.org/10.3390/foods13193076.

[27] H. Zhou, P.B. Hylemon, Bile acids are nutrient signaling hormones, Steroids. 86 (2014) 62-68. https://doi.org/10.1016/j.steroids.2014.04.016.

[28] J.Y.L. Chiang, J.M. Ferrell, Up to date on cholesterol 7 alpha-hydroxylase (CYP7A1) in bile acid synthesis, Liver Res. 4 (2020) 47-63. https://doi.org/10.1016/j.livres.2020.05.001.

[29] A. Al-Khaifi, M. Rudling, B. Angelin, An FXR Agonist Reduces Bile Acid Synthesis Independently of Increases in FGF19 in Healthy Volunteers, Gastroenterology. 155 (2018) 1012-1016. https://doi.org/10.1053/j.gastro.2018.06.038.

[30] T.Y. Jiao, Y.D. Ma, X.Z. Guo, et al., Bile acid and receptors: biology and drug discovery for nonalcoholic fatty liver disease, Acta Pharmacol Sin. 43 (2022) 1103-1119. https://doi.org/10.1038/s41401-022-00880-z.

[31] J. Martínez-García, M. Molina, L. Odriozola, et al., A minimal bile salt excretory pump promoter allows bile acid-driven physiological regulation of transgene expression from a gene therapy vector, Cell & bioscience. 12 (2022) 79. https://doi.org/10.1186/s13578-022-00803-9.

[32] H. Kuribayashi, M. Miyata, H. Yamakawa, et al., Enterobacteria-mediated deconjugation of taurocholic acid enhances ileal farnesoid X receptor signaling, Eur J Pharmacol. 697 (2012) 132-138. https://doi.org/10.1016/j.ejphar.2012.09.048.

[33] Q. Wu, X. Liang, K. Wang, et al., Intestinal hypoxia-inducible factor 2α regulates lactate levels to shape the gut microbiome and alter thermogenesis, Cell Metab. 33 (2021) 1988-2003.e1987. https://doi.org/10.1016/j.cmet.2021.07.007.

[34] J. Gillard, L.A. Clerbaux, M. Nachit, et al., Bile acids contribute to the development of non-alcoholic steatohepatitis in mice, JHEP reports : innovation in hepatology. 4 (2022) 100387. https://doi.org/10.1016/j.jhepr.2021.100387.

[35] H. Sun, Y. Guo, H. Wang, et al., Gut commensal Parabacteroides distasonis alleviates inflammatory arthritis, Gut. 72 (2023) 1664-1677. https://doi.org/10.1136/gutjnl-2022-327756.

[36] J. Zhong, X. He, X. Gao, et al., Hyodeoxycholic acid ameliorates nonalcoholic fatty liver disease by inhibiting RAN-mediated PPARα nucleus-cytoplasm shuttling, Nat Commun. 14 (2023) 5451. https://doi.org/10.1038/s41467-023-41061-8.

[37] L. Sun, Y. Pang, X. Wang, et al., Ablation of gut microbiota alleviates obesity-induced hepatic steatosis and glucose intolerance by modulating bile acid metabolism in hamsters, Acta Pharm Sin B. 9 (2019) 702-710. https://doi.org/10.1016/j.apsb.2019.02.004.

[38] C. Yang, L. Yang, Y. Yang, et al., Effects of flaxseed powder in improving non-alcoholic fatty liver by regulating gut microbiota-bile acids metabolic pathway through FXR/TGR5 mediating, Biomed Pharmacother. 163 (2023) 114864. https://doi.org/10.1016/j.biopha.2023.114864.

[39] A.M. Gómez-Pérez, P. Ruiz-Limón, J. Salas-Salvadó, et al., Gut microbiota in nonalcoholic fatty liver disease: a PREDIMED-Plus trial sub analysis, Gut Microbes. 15 (2023) 2223339. https://doi.org/10.1080/19490976.2023.2223339.

[40] M. Serino, E. Luche, S. Gres, et al., Metabolic adaptation to a high-fat diet is associated with a change in the gut microbiota, Gut. 61 (2012) 543-553. https://doi.org/10.1136/gutjnl-2011-301012.

[41] D. Mariat, O. Firmesse, F. Levenez, et al., The Firmicutes/Bacteroidetes ratio of the human microbiota changes with age, BMC Microbiol. 9 (2009) 123. https://doi.org/10.1186/1471-2180-9-123.

[42] T. Wilmanski, N. Rappaport, J.C. Earls, et al., Blood metabolome predicts gut microbiome α-diversity in humans, Nat. Biotechnol. 37 (2019) 1217-1228. https://doi.org/10.1038/s41587-019-0233-9.

[43] R.Z. Carpi, S.M. Barbalho, K.P. Sloan, et al., The Effects of Probiotics, Prebiotics and Synbiotics in Non-Alcoholic Fat Liver Disease (NAFLD) and Non-Alcoholic Steatohepatitis (NASH): A Systematic Review, Int J Mol Sci. 23 (2022) https://doi.org/10.3390/ijms23158805.

[44] Z. Wang, K.L. Lam, J. Hu, et al., Chlorogenic acid alleviates obesity and modulates gut microbiota in high-fat-fed mice, Food science & nutrition. 7 (2019) 579-588. https://doi.org/10.1002/fsn3.868.

[45] X. Zhang, O.O. Coker, E.S. Chu, et al., Dietary cholesterol drives fatty liver-associated liver cancer by modulating gut microbiota and metabolites, Gut. 70 (2021) 761-774. https://doi.org/10.1136/gutjnl-2019-319664.

[46] H. Wang, Y. Guo, W. Han, et al., Tauroursodeoxycholic Acid Improves Nonalcoholic Fatty Liver Disease by Regulating Gut Microbiota and Bile Acid Metabolism, J Agric Food Chem. 72 (2024) 20194-20210. https://doi.org/10.1021/acs.jafc.4c04630.

[47] J. Zhang, J. Zhou, Z. He, et al., Bacteroides and NAFLD: pathophysiology and therapy, Front Microbiol. 15 (2024) 1288856. https://doi.org/10.3389/fmicb.2024.1288856.

[48]M. Vacca, G. Celano, F.M. Calabrese, et al., The Controversial Role of Human Gut Lachnospiraceae, Microorganisms. 8 (2020) https://doi.org/10.3390/microorganisms8040573.

[49] L. Zhai, C. Huang, Z. Ning, et al., Ruminococcus gnavus plays a pathogenic role in diarrhea-predominant irritable bowel syndrome by increasing serotonin biosynthesis, Cell Host Microbe. 31 (2023) 33-44.e35. https://doi.org/10.1016/j.chom.2022.11.006.

[50] V. Meadows, J.M. Antonio, R.P. Ferraris, et al., Ruminococcus gnavus in the gut: driver, contributor, or innocent bystander in steatotic liver disease?, Febs j. 292 (2025) 1252-1264. https://doi.org/10.1111/febs.17327.

[51] H. Xu, F. Fang, K. Wu, et al., Gut microbiota-bile acid crosstalk regulates murine lipid metabolism via the intestinal FXR-FGF19 axis in diet-induced humanized dyslipidemia, Microbiome. 11 (2023) 262. https://doi.org/10.1186/s40168-023-01709-5.

[52] I.A. Sheikh, J. Bianchi-Smak, D. Laubitz, et al., Transplant of microbiota from Crohn's disease patients to germ-free mice results in colitis, Gut microbes. 16 (2024) 2333483. https://doi.org/10.1080/19490976.2024.2333483.

[53] N.O. Kaakoush, Insights into the Role of Erysipelotrichaceae in the Human Host, Front Cell Infect Microbiol. 5 (2015) 84. https://doi.org/10.3389/fcimb.2015.00084.

[54] Y. Chen, W. Cui, X. Li, et al., Interaction Between Commensal Bacteria, Immune Response and the Intestinal Barrier in Inflammatory Bowel Disease, Front Immunol. 12 (2021) 761981. https://doi.org/10.3389/fimmu.2021.761981.

[55] M. Meng, R. Huo, Y. Wang, et al., Lentinan inhibits oxidative stress and alleviates LPS-induced inflammation and apoptosis of BMECs by activating the Nrf2 signaling pathway, Int J Biol Macromol. 222 (2022) 2375-2391. https://doi.org/10.1016/j.ijbiomac.2022.10.024.

[56] S. Fang, T. Wang, Y. Li, et al., Gardenia jasminoides Ellis polysaccharide ameliorates cholestatic liver injury by alleviating gut microbiota dysbiosis and inhibiting the TLR4/NF-κB signaling pathway, Int J Biol Macromol. 205 (2022) 23-36. https://doi.org/10.1016/j.ijbiomac.2022.02.056.

[57] S.H. Hong, S.H. Seo, J.H. Lee, et al., The aqueous extract from Artemisia capillaris Thunb. inhibits lipopolysaccharide-induced inflammatory response through preventing NF-kappaB activation in human hepatoma cell line and rat liver, Int. J. Mol. Med. 13 (2004) 717-720.

[58] S. Li, Z. Zhang, L. Luo, et al., Millet Quinic Acid Relieves Colitis by Regulating Gut Microbiota and Inhibiting MyD88/NF-κB Signaling Pathway, Foods. 14 (2025) https://doi.org/10.3390/foods14132267.

[59] A. Alqudah, E. Qnais, O. Gammoh, et al., Exploring Scopoletin's Therapeutic Efficacy in DSS-Induced Ulcerative Colitis: Insights into Inflammatory Pathways, Immune Modulation, and Microbial Dynamics, Inflammation. 48 (2025) 575-589. https://doi.org/10.1007/s10753-024-02048-9.

[60] S.O. Vasudevan, B. Behl, V.A. Rathinam, Pyroptosis-induced inflammation and tissue damage, Semin Immunol. 69 (2023) 101781. https://doi.org/10.1016/j.smim.2023.101781.

[61] Q. Zhao, M.-Y. Dai, R.-Y. Huang, et al., Parabacteroides distasonis ameliorates hepatic fibrosis potentially via modulating intestinal bile acid metabolism and hepatocyte pyroptosis in male mice, Nature Communications. 14 (2023) https://doi.org/10.1038/s41467-023-37459-z.

[62] B. Xu, M. Jiang, Y. Chu, et al., Gasdermin D plays a key role as a pyroptosis executor of non-alcoholic steatohepatitis in humans and mice, J Hepatol. 68 (2018) 773-782. https://doi.org/10.1016/j.jhep.2017.11.040.